Investigation of the high momentum components of the nuclear wave function using hard quasielastic $A(p,2p)X$ reactions

I. Yaron, L. Frankfurt, and E. Piasetzky
School of Physics and Astronomy, Sackler Faculty of Exact Sciences, Tel Aviv University, Ramat Aviv 69978, Israel

M. Sargsian
Department of Physics, Florida International University, Miami, Florida 33199

M. Strikman
Department of Physics, Pennsylvania State University, University Park, Pennsylvania 16802
(Received 15 March 2002; published 1 August 2002)

We present a theoretical analysis of the first data for a high-energy and momentum-transfer (hard) quasielastic $A(p,2p)X$ reaction. The cross sections for this reaction are calculated within the light-cone impulse approximation based on a two-nucleon correlation model for the high-momentum component of the nuclear wave function. Nuclear effects due to modification of the bound nucleon structure as well as the soft nucleon-nucleon initial and final state interactions, with and without color coherence, have been studied in detail. The calculations show that the distribution of the bound proton light-cone momentum fraction (α) shifts towards small values ($\alpha<1$), an effect that was previously derived only within the plane wave impulse approximation. The shift is very sensitive to short-range correlations in nuclei. The calculations agree with data on the $C(p,2p)X$ reaction obtained from the EVA/AGS experiment at Brookhaven National Laboratory. The theoretical analysis of the data allows the contribution from short-range nucleon correlations to be singled out. The obtained strength of the correlations is in agreement with values previously obtained from electroproduction reactions on nuclei.

DOI: 10.1103/PhysRevC.66.024601 PACS number(s): 25.10.+s, 25.40.Ep, 25.40.Hs, 24.85.+p

I. INTRODUCTION

One of the important signatures of quark-gluon structure in the nucleon-nucleon interaction at short distances is the observed strong energy dependence ($\sim s^{-10}$) of the wide angle pp elastic differential cross section at $s \geqslant 12$ GeV^2, where s is the square of the NN center of mass (c.m.) energy. Despite the ongoing debate on the validity of perturbative QCD in this energy region [1–3] or the debate on the relevance of a particular mechanism of subnucleon interaction (i.e., quark-interchange [4–6], three-gluon exchange [7,8], reggeon-type contribution [9]), it is commonly accepted that the power-law s dependence of the elastic cross section signals the onset of the hard dynamics of the quark-gluon interaction.

In this paper we address the question of what happens when wide angle pp scattering takes place inside the nucleus, i.e., the incident proton is scattered off a bound proton. If this reaction has the same $\sim s^{-10}$ energy dependence as that of the cross section of free pp scattering, one may expect that the incoming proton will favorably scatter off a bound proton with larger initial momentum aligned in the direction of the incoming proton [10,11]. This kinematic condition corresponds to pp scattering with a smaller s and therefore a larger scattering cross section. Thus, if nuclear effects do not alter the genuine s dependence of the pp cross section, the high-momentum-transfer $p+A \rightarrow p+p+X$ reaction preferably selects the high-momentum components of the nuclear wave function.

Due to the short-range nature of the strong interaction, the high internal momentum in the nucleus is generated mainly by short-range NN correlations. Therefore, at sufficiently high energies and high-momentum transfers one expects to be able to probe the short-range properties of the nucleus.

In Refs. [10,11], the authors calculated the cross section of high-momentum-transfer $A(p,2p)X$ reactions within a plane wave impulse approximation (PWIA) and observed a strong sensitivity to the high-momentum components of the nuclear wave function. Motivated by the recent measurements of high-momentum transfer pA reactions at Brookhaven National Laboratory (BNL) [12] we carried out a detailed analysis of the high-momentum transfer $A(p,2p)X$ reaction, investigating specifically the competing nuclear effects, not discussed previously. These effects may obscure the observed sensitivity found in PWIA [11]. Our main goal is to see whether these reactions probe short-range correlations (SRC) and to study their sensitivity to the dynamical structure of these correlations.

The structure of the paper is as follows: In Sec. II we outline the basic theoretical framework for the calculation of the high-energy wide angle quasielastic $A(p,2p)X$ reaction. We also discuss the nuclear effects which can compete with the expected signatures of scattering from SRC. In Sec. III we present the predictions of the model presented in Sec. II. Section IV describes briefly the EVA experiment at BNL. The calculations are compared with the data obtained in that experiment in Sec. V. Section VI summarizes the results of our study.

II. THE BASIC THEORETICAL FRAMEWORK

In quasielastic (QE) scattering a projectile is elastically scattered from a single bound ''target'' nucleon in the

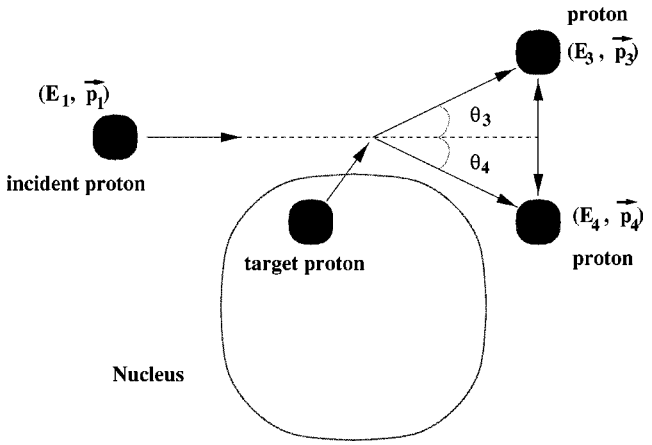

FIG. 1. The kinematics for quasielastic $A(p,2p)X$ scattering.

nucleus while the rest of the nucleus acts as a spectator. A schematic presentation of $(p,2p)$ QE scattering is given in Fig. 1.

A. Kinematics

$p_A=(E_A,\vec{p}_A)$, $p_1=(E_1,\vec{p}_1)$, $p_3=(E_3,\vec{p}_3)$, $p_4=(E_4,\vec{p}_4)$, $p_R=(E_R,\vec{p}_R)$ are the four-momenta of the target nucleus, the incoming proton, the scattered proton, the ejected proton and the recoil nucleus, respectively. For simplicity we do not show p_A and p_R in Fig. 1. Using the notations defined in the figure, the Mandelstam variables are

$$s=(p_3+p_4)^2, \quad t=(p_1-p_3)^2. \tag{1}$$

The primary high-momentum-transfer process in the $A(p,2p)X$ quasielastic reaction is hard pp elastic scattering. Since the general predictions are based on the implication of the strong s dependence ($\sim 1/s^{10}$) of the hard elastic pp cross section we will limit our calculations to high-energy and high-momentum-transfer kinematics where that dependence is observed experimentally. Thus, our calculations are limited to $s \gtrsim 12$ GeV^2 and $\theta_{\text{c.m.}} \sim 90°$.

The missing energy (E_m) for $A(p,2p)X$ is defined by $E_m=E_1+E_A-E_3-E_4-E_{A-1}$. The available high-energy $A(p,2p)X$ data have a missing energy resolution of about 240 Mev [12]. Therefore, the calculations with which we compare with the data are integrated over a wide range of missing energies. This integration simplifies the calculations, as discussed below.

B. Plane wave impulse approximation

A clear interpretation of the quasielastic measurements is possible in PWIA. Within this approximation, it is possible to separate nuclear properties from the reaction mechanism.

In high-energy scattering the reaction evolves near the light cone $\tau=t-z\sim 1/(E+p_z) \ll t+z$, where z is the direction of the incident proton and E and p_z are the energy and leading longitudinal momentum of the high-energy particles involved in the scattering. Thus, it is natural to describe the reaction in the light-cone reference frame (similar to high-energy deep-inelastic scattering from a hydrogen target [13]).

Within the light cone PWIA, the cross section of the quasielastic $A(p,2p)X$ reaction can be expressed as a convolution of the elementary elastic pp scattering cross section off a bound nucleon and the four-dimensional light-cone spectral function [10],

$$\frac{d^6\sigma}{(d^3p_3/2E_3)(d^3p_4/2E_4)} = \sum_Z \frac{1}{4j_{pA}} \frac{|M_{pp}|^2}{(2\pi)^2} \frac{P_A(\alpha,p_t^2,p_{R+})}{\alpha^2}$$
$$= \sum_Z \frac{2}{\pi}\sqrt{s^2-4m^2s}\,\frac{d\sigma}{dt}^{pp}(s,t) \times \frac{P_A(\alpha,p_t^2,p_{R+})}{A\alpha}, \tag{2}$$

where

$$p_2=p_3+p_4-p_1, \quad p_t=p_3^t+p_4^t,$$
$$\alpha=\alpha_4+\alpha_3-\alpha_1, \quad \alpha_i=A\frac{p_{i-}}{P_{A-}}\equiv A\frac{E_i-p_i^z}{E_A-P_A^z}. \tag{3}$$

The superscripts "t" and "z" denote the transverse (x,y) and longitudinal directions with respect to the incoming proton momentum $\vec{p}_1$. The "+" and "−" indices denote the energy and longitudinal components of four-momenta in the light cone reference frame.[1] The variable α, as defined, describes the light cone momentum fraction of the nucleus carried by the target nucleon, normalized in such a way that a nucleon at rest has $\alpha=1$. j_{pA} is the invariant flux with respect to the nucleus, while M_{pp} and $(d\sigma/dt)^{pp}$ are the invariant amplitude and cross section for elastic pp scattering.

The light cone spectral function represents the probability of finding the target nucleon with the light-cone momenta (α,p_t) times the probability that the residual nuclear system has a momentum component $p_{R+}=E_R+p_R^z$. The spectral function is normalized as follows [10]:

$$\int \frac{p_{A-}}{2A} P_A(\alpha,p_t^2,p_{R+})\frac{d\alpha}{\alpha}d^2p_t dp_{R+}=A. \tag{4}$$

C. The light-cone spectral function

The integration over a wide range of the missing energy allows us to use the following approximations for the spectral function.

For target proton momenta below the Fermi sea ($p_2 < p_{Ferm} \sim 250$ MeV/c) we use the nonrelativistic limit of the light-cone spectral function [14,10],

$$P_A(\alpha,p_t^2,p_{R+}) \approx \tfrac{1}{2} n(p_2)\,\delta(p_{R+}-[\sqrt{M_{A-1}^2+p_2^2}-p_2^z]), \tag{5}$$

[1]Since z direction is chosen as the direction of incoming proton momentum, the "−" component corresponds to the light-cone longitudinal momentum.

where $\alpha \approx 1 - p_2^z/m$ and $\vec{p}_2 = \vec{p}_3 + \vec{p}_4 - \vec{p}_1$ is the missing momentum of the reaction. $n(p)$ is the momentum distribution of nucleons calculated within the mean field approximation.

For the momentum range of ($p_{\rm Ferm} < p_2 < 0.7$ GeV/c) we assume the dominance of the two-nucleon short-range correlations, which allows us to model the spectral function as follows [10,15]:

$$P_A(\alpha, p_t^2, p_{R+}) \approx \int \frac{A^2}{2p_{A-}} a_2(A) \rho_2^n \left[\frac{2\alpha}{(A-\beta)}, \left(\vec{p}_t + \frac{\alpha}{(A-\beta)} \vec{p}_{(A-2)t} \right)^2 \right] \rho_{A-2}(\beta, p_{(A-2)t}^2) \times \delta\left(p_{R+} - \frac{m^2 + (\vec{p}_{(A-2)t} + \vec{p}_t)^2}{m(A-\alpha-\beta)} - \frac{M_{A-2}^2 + p_{(A-2)t}^2}{m\beta} \right) \frac{d\beta}{\beta} d^2 p_{(A-2)}^t, \quad (6)$$

where $(\beta, p_{(A-2)t}^2)$ and ρ_{A-2} are the light-cone momentum and the density matrix of the recoiling $(A-2)$ system. The parameter $a_2(A)$ is the probability of finding two-nucleon correlations in the nucleus A and ρ_2^n is the density matrix of the correlated pair which we set equal to the light-cone density matrix of the deuteron [14],

$$\rho_2^n(\alpha, p_t^2) = \frac{\Psi_D^2(k)}{2-\alpha} \sqrt{m^2 + k^2}, \qquad k = \sqrt{\frac{m^2 + p_t^2}{\alpha(2-\alpha)} - m^2}; (0 < \alpha < 2). \quad (7)$$

Note that the factorization of the nuclear density matrix into the product of the correlation and $(A-2)$ density matrices is specific for the short-range two-nucleon correlation approximation. In this approximation it is assumed that the singular character of the NN potential at short distances (existence of repulsive core) defines the main structure of the nucleon momentum distribution in SRC and that it is less affected by the collective interaction with the $(A-2)$ nuclear system. Note that the expression in Eq. (7) is the light-cone analog of the approximated spectral function in Ref. [16], where the validity of the two-nucleon correlation approximation was demonstrated by comparing the nonrelativistic analog of Eq. (6) with the exact calculations of the spectral function of ^{3}He and infinite nuclear matter.

To obtain the density matrix of the recoiling $(A-2)$ system, additional physical assumptions are required. However, the fact that we are interested in the cross section integrated over a wide range of missing energies, allows us to simplify Eq. (6) by neglecting the momentum of the recoiling $(A-2)$ system (SRC at rest approximation),

$$\rho_{A-2}(\beta, p_{(A-2)t}^2) = (A-2)\, \delta(A-2-\beta)\, \delta(p_{(A-2)t}^2). \quad (8)$$

Inserting Eq. (8) into Eq. (6) one obtains the following expression for the light-cone spectral function in the high missing momentum range,

$$P_A(\alpha, p_t^2, p_{R+}) \approx \frac{A^2}{2p_{A-}} a_2(A) \rho_2^n(\alpha, p_t^2) \times \delta\left(p_{R+} - \frac{m^2 + p_t^2}{m(2-\alpha)} - M_{A-2} \right). \quad (9)$$

It is worth noting that the above approximation is justified by the fact [16] that it correctly predicts the position of the maximum in the missing energy distribution at fixed values of missing momentum. Therefore, in a regime in which the integration over the wide range of missing energies is allowed, Eq. (9) represents a valid approximation of nuclear spectral functions in the domain of the large values of bound nucleon momenta. The same model was also used to describe inclusive nucleon and pion production in forbidden kinematics for scattering off a free nucleon [10,14], and electroproduction [14,15] reactions from nuclei at $x_{\rm Bjorken} > 1$ and $Q^2 \geq 1$ GeV^2.

D. Proton-proton elastic scattering cross section

The next quantity that is needed to calculate the quasielastic $A(p,2p)X$ cross section in Eq. (2) is the differential cross section of pp elastic scattering. For $s \geq 12$ GeV^2 we use the phenomenological parametrization of the free pp elastic cross section. We assume a combination of s parametrization at 90° presented in Ref. [41] and $\theta_{\rm c.m.}$ parametrization in the form suggested in Ref. [18],

$$\frac{d\sigma}{dt}^{pp} = 45.0 \frac{\mu{\rm b}}{{\rm sr\ GeV}^2} \left(\frac{10}{s} \right)^{10} (1 - \cos\theta_{\rm c.m.})^{-4\gamma} \times \left[1 + \rho_1 \sqrt{\frac{s}{\rm GeV}}^2 \cos\phi(s) + \frac{\rho_1^2}{4} \frac{s}{\rm GeV^2} \right] F(s, \theta_{\rm c.m.}), \quad (10)$$

where $\rho_1 = 0.08$, $\gamma = 1.6$ and $\phi(s) = \pi/0.06 \ln(\ln[s/(0.01\ {\rm GeV}^2)])^{-2}$. The function $F(s, \theta_{\rm c.m.})$ is used for further adjustment of the phenomenologically motivated parametrization of the data at $60° \leq \theta_{\rm c.m.} \leq 90°$ [19].

E. Calculation of the α-dependence of the cross section in PWIA

Our main objective is to study the α dependence of the $A(p,2p)X$ quasielastic cross section at large fixed c.m. angles and high-momentum transfers. The reason for this choice is twofold: first, the α dependence naturally expresses the sensitivity of the $A(p,2p)X$ cross section to the high-momentum component of the nuclear wave function; second, the α variable is not sensitive to soft initial and final state reinteractions of energetic protons with target nucleons (see Sec. II F 2). Thus the α distribution will largely reflect the distribution of the nucleon within the SRC without substantial modification due to initial and final state interactions.

In Fig. 2 we present the α dependence of the ^{12}C$(p,2p)X$ cross section calculated within PWIA (Sec. II B) for different values of incoming proton momenta. Here the c.m. angle of the $pp \to pp$ scattering is restricted to 90°±5°. The calcula-

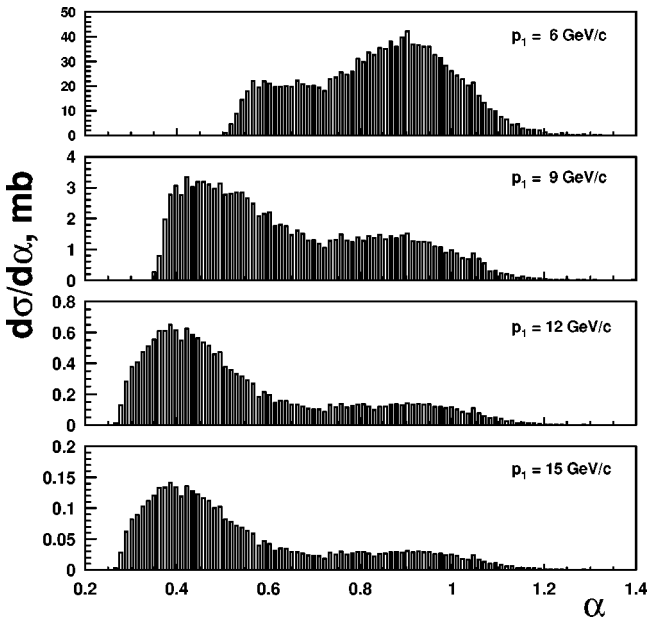

FIG. 2. PWIA calculation of the α dependence of the $^{12}C(p,2p)X$ cross section at different values of incident proton momenta.

tion is done for ^{12}C using a harmonic oscillator momentum distribution for $n(k)$ in Eq. (5) and a high-momentum tail of the deuteron wave function, with Paris potential in Eq. (7), with $a_2(^{12}C)=5$.

Elastic p scattering on a proton at rest corresponds to $\alpha=1$. As can be seen from Fig. 2, most of the strength is at $\alpha<1$ which corresponds to scattering off a proton with momenta in the direction of $\vec{p}_1$. This is a quantitative illustration of the discussion in the Introduction: the pp cross section on bound protons scales with the total pp c.m. energy as $\sim(s\alpha)^{-10}$, therefore the $A(p,2p)X$ cross section is dominated by smaller α.

One can clearly observe a double peak structure in the α distributions. The first peak, closer to $\alpha=1$, is due to scattering off a proton in the Fermi sea Eq. (5). The other peak, at an even lower α value, is due to the scattering off the SRC Eq. (6). As the incoming energy increases, one can see the shift of the strength of the distribution to lower α range which shows the dominance of the incoming proton scattering off a target protons with high Fermi momenta aligned in the direction of the beam. This shift shows the onset of the regime where one expects to probe short-range nucleon correlations in the nucleus. This picture demonstrates the selectivity of hard $A(p,2p)X$ reactions to the large values of the bound nucleon momenta in the nucleus, predicted originally in Refs. [10,11].

F. Competing nuclear effects

The PWIA calculation discussed above uses the pp hard scattering cross section parametrization [Eq. (10)] for scattering off a free proton. The two nuclear effects that can obscure the α dependence expected within PWIA are the modification of the bound protons in nuclei and the initial and final state interactions of incoming and scattered protons.

1. Nuclear medium modification of bound protons

We consider possible binding modifications of the nucleon structure, which are consistent with the observation of the modification of deep inelastic (DIS) nucleon structure functions measured in lepton-nucleus scattering, a phenomenon known as the ''EMC effect'' [20]. One of the mechanisms that describes the observed modification of DIS structure function is the suppression of pointlike configurations (PLC) in a bound nucleon as compared to a free nucleon [21,10,22].

Pointlike configurations are small sized partonic configurations in the nucleons which, due to the color screening, are weakly interacting objects. In the color screening model of Refs. [21,10], the binding of the nucleonic system causes a suppression of the nucleon's PLC component. This suppression does not lead to a noticeable change in the average characteristics of a nucleon in the nucleus. However, it is sufficient to account for the observed EMC effect in DIS scattering from nuclei. Since high-momentum transfer pp elastic scattering is mainly due to the scattering off a PLC in the proton, the expected suppression of PLC will reduce the cross section of pp scattering from bound protons. This suppression can be estimated by multiplying the free pp cross section of Eq. (10) by the factor [21]

$$\delta(k,t)=\left[1+\Theta(t_0-t)\left(1-\frac{t_0}{t}\right)\frac{\frac{k^2}{m_p}+2\epsilon_A}{\Delta E}\right]^{-2}, \quad (11)$$

where $\epsilon_A\approx 8$ MeV is the average nuclear binding energy and $\Delta E\approx 0.6-1$ GeV is a parameter that characterizes a typical excitation of the bound nucleon. The t dependence in Eq. (11) is due to the fact that in the wave function of a nucleon the PLC dominates at high values of the momentum transfer [23] ($-t_0\approx 2$ GeV^2). As follows from Eq. (11), the $\delta(k,t)$ correction tends to reduce the expected α shift shown in Fig. 1, since it introduces an additional α^l ($l\sim 2-3$) dependence, which softens the $(s\alpha)^{-10}$ dependence of the pp cross section in Eq. (2). Note that a similar suppression is expected within the rescaling model of the EMC effect [24–26]. On the other hand, in a number of models of the EMC effect, such as pion and binding models (for review see Ref. [10]) the shift to $\alpha<1$ is stronger than in the multinucleon calculation [11,26]. Thus, our estimate within the color screening model can be considered as an upper limit for suppression due to binding nucleon modification.

Using Eqs. (2) and (9)–(11), the calculated cross sections as a function of α are shown in Fig. 3. As Fig. 3 shows, the medium modification effect suppresses the cross section in the smaller α region, where the cross section is dominated by the scattering from deeply bound (SRC) protons in which the suppression of PLC is larger. However, the suppression does not diminish the downward shift of the α distribution. It would require very unreasonable modifications of the bound

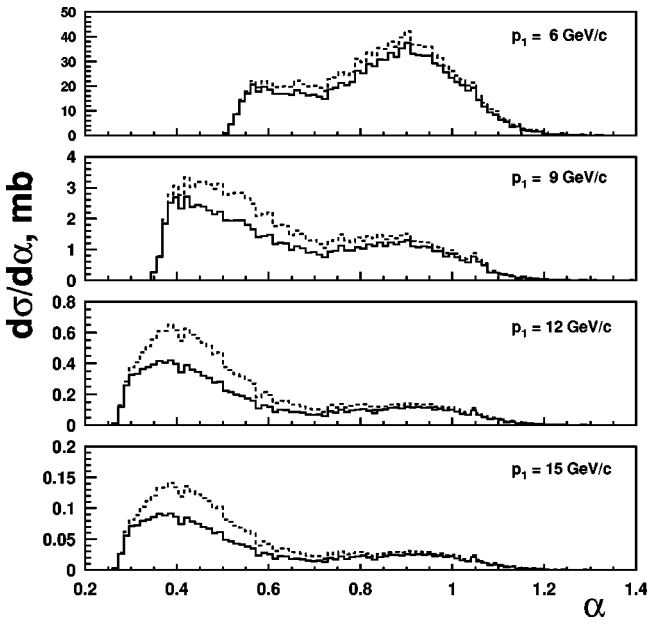

FIG. 3. The α dependence of the cross section for different values of incident proton momentum. Dashed line, PWIA; solid line, with EMC effects discussed in the text. The kinematics are the same as for Fig. 2.

nucleon structure (contradicting the EMC effects in DIS) to eliminate the α shift (to the $\alpha<1$ region) completely.

2. The effect of the initial and final state interactions

The major nuclear effect that can obscure the information on SRC is the contribution of initial and final state interactions (ISI, FSI) of the incident and outgoing protons in the nuclear medium. Since the momenta of the incoming and the two outgoing protons are above a few GeV/c, one can calculate these rescatterings in eikonal approximation.

For rescattering from uncorrelated nucleons with momenta $0.8<\alpha<1.2$ and $p_t \leqslant p_{\rm Ferm}$, we apply the conventional Glauber approximation. This is justified since under these conditions the spectator nucleons can be considered as stationary scatterers. Because of the integration over a large range of missing energies we can further simplify the calculations by using the probabilistic approximation of Ref. [27].

The above approximation cannot be used for the bound protons in SRC (which have a large value of Fermi momentum). There the spectator nucleon cannot be treated as a stationary scatterer and therefore the Glauber approximation is not valid (see, e.g., Ref. [28]). To calculate ISI/FSI in this case, we assume that the first rescattering most probably happens with the partner nucleon in the SRC. Indeed, as was demonstrated in Ref. [15], because of the large virtuality of the interacting nucleon in SRC the distance of the first soft reinteraction after the point of hard interaction is less than 1 fm and it decreases as t and p_2 increase. Within the two-nucleon correlation model one can account for the soft rescatterings in the SRC using the calculation of the $d(p,2p)n$ reaction in generalized eikonal approximation (GEA) [28,29]. Within GEA we calculate the single rescatterings of the incoming and knocked-out protons with the correlated

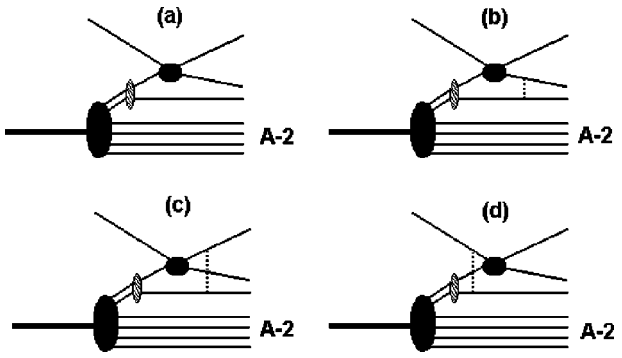

FIG. 4. Diagrams describing PWIA (a), final (b,c), and initial (d) state reinteractions for two-nucleon correlations.

nucleon [Figs. 4(b–d)]. The main feature of the GEA is that it takes into account the nonzero values of the spectator momentum (it does not treat the spectator as a stationary scatterer as is done in the conventional eikonal approximation). This feature is especially important in the SRC region as the correlated nucleon momenta are large and cannot be neglected.

Within GEA, the effect of the rescatterings in the SRC (in the range of $\alpha<0.8$ or $\alpha>1.2$) can be accounted for by introducing a correction factor κ that multiplies the SRC spectral function of Eq. (9). We define κ as follows:

$$\kappa=\frac{|F_a+F_b+F_c+F_d|^2}{|F_a|^2}, \tag{12}$$

where F_a is the PWIA amplitude, and F_b, F_c, and F_d are the single rescattering amplitudes corresponding to $p+(NN)_{SRC}\rightarrow p+N+N$ scattering shown in Fig. 4. To obtain the F's, we use the rescattering amplitudes for the $d(p,pp)n$ reaction calculated in Ref. [29],

$$F_{(j)}=-\frac{(2\pi)^{3/2}}{4i}A_{pp}^{hard}(s,t)\int\frac{d^2k_t}{(2\pi)^2}f^{pN}$$
$$\times(k_t)[\psi_d^{\mu}(\tilde{p}_s^{(j)})-ni\psi'^{\mu}(\tilde{p}_s^{(j)})], \tag{13}$$

where $j(n)=b(1),c(1),d(-1)$. A_{pp}^{hard} is the amplitude of the pp hard scattering which, within the factorization approximation, cancels in κ. f^{pN} is the amplitude of a small angle (soft) pN scattering. ψ_d is the deuteron wave function and ψ' accounts for the distortion due to FSI (see Ref. [29]).

For higher order rescatterings we have applied the probabilistic approximation of Ref. [27] which we used already for small Fermi momenta. This is justified since in the kinematics of two-nucleon SRC the second and higher order rescatterings happen outside the SRC. It is worth noting that the error from the last approximation is rather small since, for intermediate size nuclei ($A\sim12-16$), the overall contribution of higher order rescatterings in the considered kinematics of the $A(p,2p)X$ reaction is small (a few percent as compared with the single rescattering contribution [27]).

It is important to emphasize that, for reinteractions with uncorrelated nucleons at high energies, there exists an approximate conservation law for the light-cone momenta of

interacting particles [28,30]. Namely, for energetic particles, small angle soft reinteractions do not change the α distribution.

To demonstrate this, let us consider the propagation of a fast nucleon with momentum $p_1=(E_1,p_1^z,0)$ through the nuclear medium. After the small angle reinteraction with a nucleon of momentum $p_2=(E_2,p_2^z,p_2^t)$, the energetic nucleon still maintains its high momentum and leading z direction having now a momentum $p_1'=(E_1',p_1^{z'},p_1^{t'})$ with $\langle(p_1^{t'})^2\rangle/(p^{z'})^2\ll 1$. The other nucleon momentum after the collision is $p_2'=(E_2',p_2^{z'},p_2^{t'})$. The energy momentum conservation for this scattering allows us to write for the "α" component

$$\alpha_1+\alpha_2=\alpha_1'+\alpha_2'\equiv\frac{p_{1-}}{m}+\frac{p_{2-}}{m}=\frac{p_{1-}'}{m}+\frac{p_{2-}'}{m}. \quad (14)$$

The change of the α_2 ("$-$") component due to rescattering can be obtained from Eq. (14),

$$\Delta\alpha_2\equiv\frac{\Delta p_{2-}}{m}=\frac{p_{2-}-p_{2-}'}{m}=\frac{p_{1-}'-p_{1-}}{m}\ll 1, \quad (15)$$

which means

$$\alpha_2'\approx\alpha_2. \quad (16)$$

In Eq. (15) we use the approximations $p_{1-}'/m, p_{1-}/m\ll 1$ which are well satisfied in small angle reinteractions since $\langle(p_1^{t'})^2\rangle/(p^{z'})^2\ll 1$. Thus, with the increase of the incident energy a new approximate conservation law is emerging: α_2 is conserved by ISI/FSI. The uniqueness of the high-energy rescattering lies in the fact that, although both the energy and the momentum of the nucleons are changed by the rescattering, the combination $(E_2-p_2^z)$ is almost not affected. In the same way, the rescattering of the incoming and two outgoing protons in the $(p,2p)$ reaction conserves the reconstructed α component of the target proton. Therefore, the α distribution measured in $A(p,2p)X$ reaction reflects well the original α distribution of the target proton in the nucleus. A numerical estimate of this conservation will be presented in the following section.

To complete the discussion on ISI/FSI we should mention that for incident proton momenta exceeding 6–9 GeV/c, the Glauber approximation overestimates the absorption of protons for the data of Refs. [31,32]. This overestimate is attributed to the color transparency (CT) phenomenon (see, e.g., Refs. [33–36]), in which it is assumed that the hard $pp\to pp$ primary process in the $A(p,2p)X$ reaction is dominated by the interaction of protons in pointlike qqq configurations. As a result, immediately before and after the hard interaction the color neutral PLC has a diminished strength for ISI/FSI reinteraction. Since the PLC is not an eigenstate of the QCD Hamiltonian (free nucleons have a finite size) the interaction strength will evolve to the normal hadronic interaction strength parallel to the evolution of PLC to the normal hadronic size during the propagation of the fast proton in the nuclear medium. We estimate the charge transfer (CT) effect within the quantum diffusion model of Ref. [37]. This model that describes the data [31] reasonably well [23] assumes the following amplitude for the PLC-N soft interaction:

$$f^{PLC,N}(z,k_t,Q^2)=i\sigma_{tot}(z,Q^2)e^{b/2t}\frac{G_N(t\sigma_{tot}(z,Q^2)/\sigma_{tot})}{G_N(t)}, \quad (17)$$

where $b/2$ is the slope of elastic NN amplitude, $G_N(t)$ $[\approx(1-t/0.71)^2]$ is the Sachs form factor and $t=-k_t^2$. The last factor in Eq. (17) accounts for the difference between elastic scattering of PLC and average configurations, using the observation that the t dependence of $d\sigma^{h+N\to h+N}/dt$ is roughly that of $\sim G_h^2(t)G_N^2(t)$ and that $G_h^2(t)\approx\exp(R_h^2t/3)$, where R_h is the rms radius of the hadron.

In Eq. (17), $\sigma_{tot}(l,Q^2)$ is the effective total cross section for the PLC to interact at distance l from the hard interaction point and σ_{tot} is the pN total cross section. The quantum diffusion model [37] predicts

$$\sigma_{tot}(Q^2)=\sigma_{tot}\left\{\left[\frac{z}{l_h}+\frac{\langle r_t(Q^2)^2\rangle}{\langle r_t^2\rangle}\left(1-\frac{z}{l_h}\right)\right]\Theta(l_h-z)+\Theta(z-l_h)\right\}, \quad (18)$$

where $l_h=2p_f/\Delta M^2$, with $\Delta M^2=0.7$–1.1 GeV^2. Here $\langle r_t(Q^2)^2\rangle$ is the average squared transverse size of the configuration produced at the interaction point. In several realistic models discussed in Ref. [38] it can be approximated as $\langle r_t(Q^2)^2\rangle/\langle r_t^2\rangle\sim 1$ GeV$^2/Q^2$ for $Q^2\geqslant 1.5$ GeV^2. Note that due to expansion of the PLC, the results of the calculations are rather insensitive to the value of this ratio whenever it is much less than unity. For numerical calculations we assumed $\Delta M^2\approx 0.7$ GeV^2 which was chosen to describe the nuclear transparencies from $A(p,2p)X$ [31] and $A(e,e'p)X$ [39] experiments (see comparisons in Ref. [23]).

In Fig. 5 we compare the prediction of the quantum diffusion model for the nuclear transparency T with the data of the EVA experiment [12,32]. The transparency T is defined as the ratio of the $A(p,2p)X$ cross section calculated using PWIA, color screening and rescattering effects, to the cross section calculated within PWIA only. The comparison shows that there is fair agreement with the data up to 9 GeV/c incoming proton momenta. (Note that one expects the probabilistic model of rescattering to work within 20% accuracy.) The decrease of the experimental values of transparency in the $p_1>9$ GeV/c region can be understood in terms of the interplay of the hard and soft components in the amplitude of high-momentum-transfer pp scattering [41,17] which is not incorporated in the current calculations. Since, in the further analysis, we will concentrate on incoming proton momenta $5.9\leqslant p_1\leqslant 7.5$ GeV/c where this interplay does not play a role, we will use the simple formulas of Eqs. (17) and (18) for numerical estimates. The detailed analysis of the energy dependence of the nuclear transparency T will be presented elsewhere.

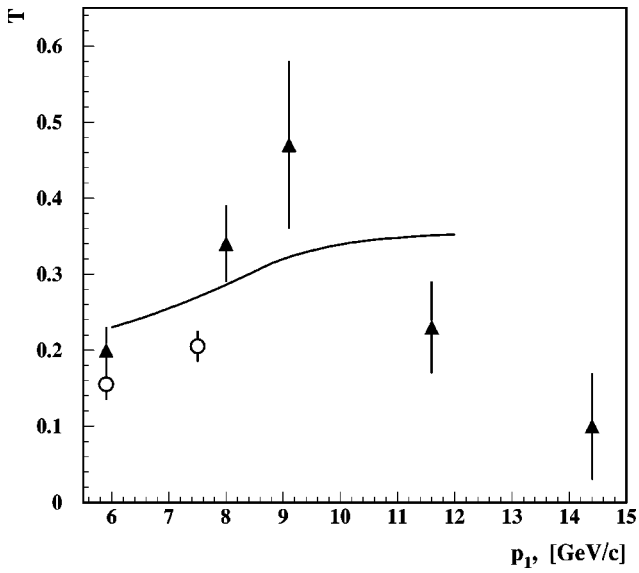

FIG. 5. The p_1 dependence of the transparency T calculated within quantum diffusion model. Data marked by triangles and circles are from Refs. [32] and [40], respectively.

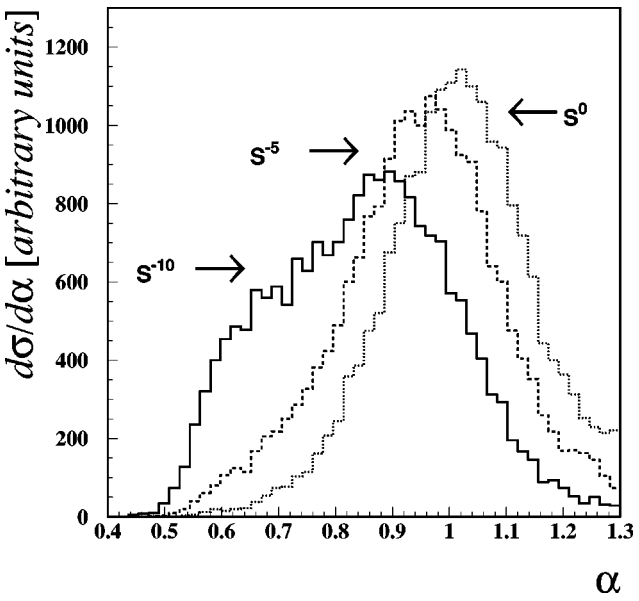

FIG. 6. The α dependence of the $A(p,2p)X$ cross section for different assumed s dependences of the hard elastic pp scattering cross section.

III. RESULTS OF THE MODEL

In this section we discuss the results of the model presented in Sec. II for several nuclear observables that can be measured in the $A(p,2p)X$ reaction. We are particularly interested in two kinds of information: how the substructure of high-momentum-transfer pp scattering reveals itself in the nuclear reaction and the information one can obtain about short-range nuclear structure. For numerical estimates we apply the kinematics of the EVA experiment [12]. Because of the multidimensional character of the kinematical restrictions, the Monte Carlo method was used to perform the calculations. Furthermore, we will present the cross sections in arbitrary units since we are interested mainly in the shapes of the α and p_t dependences of the $A(p,2p)X$ cross section.

A. How the quark substructure of hard *pp* scattering is reflected in the nuclear observables

Since the cross section for the high-momentum-transfer scattering of incoming proton off a bound proton at fixed and large $\theta_{\text{c.m.}} \sim 90°$ is roughly proportional to $(\alpha s)^{-10}$ [see Eqs. (2)–(10)], an observation that reflects the sensitivity of $A(p,2p)X$ reaction to the high-momentum component of the nuclear wave function is the shift of the α spectrum to lower α values (see Figs. 2 and 3). To see whether this sensitivity persists for the EVA kinematics, in Fig. 6 we represent the α dependence of the $A(p,2p)X$ reaction cross section assuming different s dependences of the cross section for hard $p+p \rightarrow p+p$ scattering. These calculations are merely to illustrate the connection between the s dependence and the α shift. Figure 6 confirms that the larger the negative power of s dependence for the hard pp scattering, the larger the average longitudinal momentum of the interacting bound nucleon ($\alpha<1$).

As a result of the α shift the total longitudinal momentum of the final outgoing protons is larger than the initial longitudinal momentum p_1. One can characterize this excess through the variable

$$x = \frac{p_3^z + p_4^z}{p_1}, \tag{19}$$

which will increase as the power of the hard pp scattering cross section increases. In Fig. 7 we show the calculated x dependence of the cross section for different assumed s dependences. The expected shift to the higher x (lower α) is clearly seen in Fig. 7. The x distribution for quasielastic $C(p,2p)X$ reactions peaks at $x<1$, if one assumes no s de-

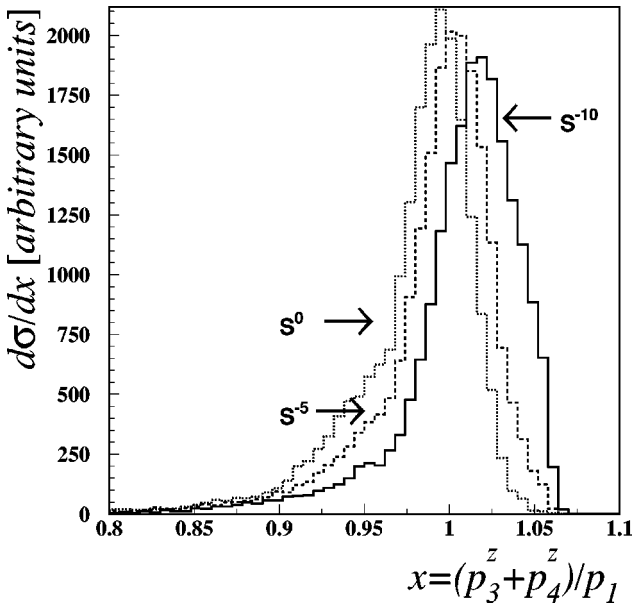

FIG. 7. The x dependence of the cross section for different hard elastic pp scattering power laws.

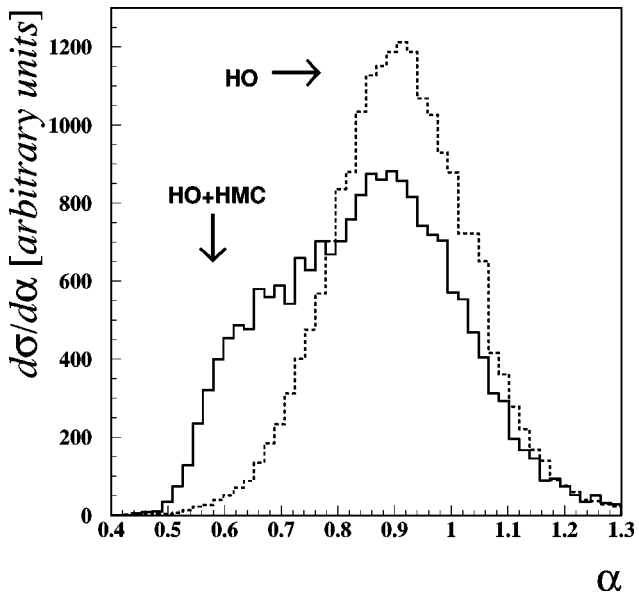

FIG. 8. The α dependence of the cross section calculated for two models of the nuclear wave functions. HO is harmonic oscillator and HO+HMC corresponds to the short-range correlation model of Sec. II C. The $A(p,2p)X$ cross section is calculated within PWIA at $p_1=6$ GeV/c and $\theta_{\text{c.m.}}=90°$.

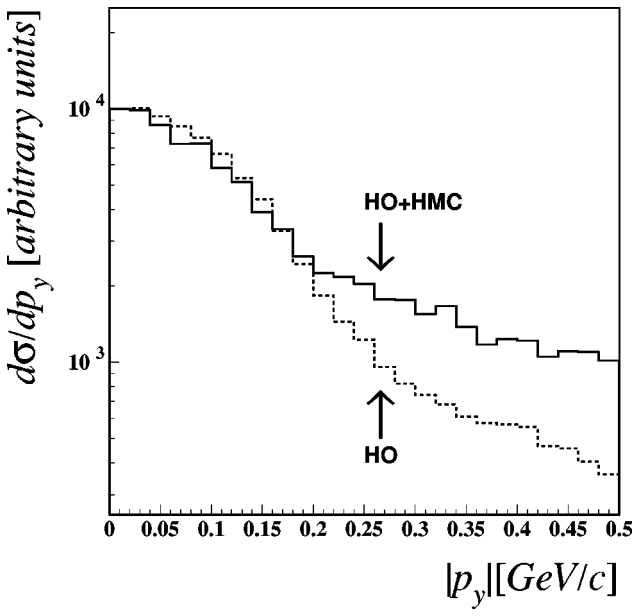

FIG. 9. The p_y dependence of the cross section for the two models of nuclear wave functions described in the text. The kinematics of the calculations and notations are the same as in Fig. 8.

pendence of the elementary $p+p\rightarrow p+p$ reaction. As the dependence on s increases, the peak is shifted towards $x>1$ which represents the nuclear ''boosting'' effect: the outgoing protons have more longitudinal momentum than the incoming momentum. This effect is reminiscent of subthreshold production in nuclei, in which a very low available energy in the nuclear medium can cause considerable changes in the cross section of the reaction.

B. Sensitivity to short-range correlations in nuclei

The next question that we would like to address is the sensitivity of the α shift to the existence of high-momentum components in the nuclear ground state wave function. To asses this sensitivity we calculate the cross sections of the $A(p,2p)X$ reaction using two models for the nuclear wave function: a harmonic oscillator (HO) model and the two-nucleon SRC model for high-momentum components (HMC) of the nuclear wave function, described in Sec. II C (HO+HMC). In Fig. 8 we present the α dependence of the $^{12}\text{C}(p,2p)X$ cross section calculated within PWIA at $p_1=6$ GeV/c and $\theta_{\text{c.m.}}=90°$ using these two models.

As Fig. 8 shows, even at the moderate energy of $p_1=6$ GeV/c, the α dependence has substantial sensitivity to the high-momentum structure of the nuclear wave function. Thus, the measured cross section at small α will allow us to obtain the characteristics of the high-momentum tail of the wave function.

In Fig. 9, we show the results of the PWIA calculations for the transverse momentum distribution of the cross section of $^{12}\text{C}(p,2p)X$ reaction. It also exhibits a sensitivity to the high-momentum part of the nuclear wave function. However, as will be shown below, unlike the α distribution the transverse momentum distribution is strongly distorted due to the initial and final state interactions. Note that hereafter, for the transverse missing momentum distribution, we will consider only the p_y component of p_t, where $\hat{y}=[\hat{x}\times\hat{z}]$ and (xz) defines the scattering plane of the incoming proton. This restriction on p_y is related to the fact that the experimental data has a better resolution for the y component of missing momentum.

C. The effect of initial and final state interactions

As was discussed in Sec. II [see Eq. (15)], one expects that the soft rescatterings with uncorrelated nucleons at high energies will conserve the α parameter of interacting nucleons. Thus the measured α_2 distribution of $A(p,2p)X$ cross section is not affected strongly by the ISI/FSI and will reflect the original α distribution of the target proton in the nucleus.

In Fig. 10 we show the results for the p_2 and α distributions of the $^{12}\text{C}(p,2p)X$ differential cross section at $p_1=6$ GeV/c and $\theta_{\text{c.m.}}=90°$. The dashed lines correspond to the PWIA prediction, thus representing the ''true'' momentum distribution of the bound nucleon. The solid lines represent the calculation including ISI/FSI. In the latter case p_2 and α are reconstructed through the momenta of the incoming (p_1) and outgoing protons (p_3,p_4), as it was done in the experiment (see Sec. IV). Notice the effect of the ISI/FSI on the p_2 distribution versus the effect of the same ISI/FSI on the α distribution. As we mentioned before, both the reconstructed energy and the momentum of the target proton are modified by the rescattering, but their linear combination, α, is almost unchanged.

Finally, in Fig. 11 we show the transverse momentum distribution (p_y) calculated for the same kinematics as in Fig. 10. Figure 11 shows substantial ISI/FSI effects on the p_y distribution for both calculation with and without color trans-

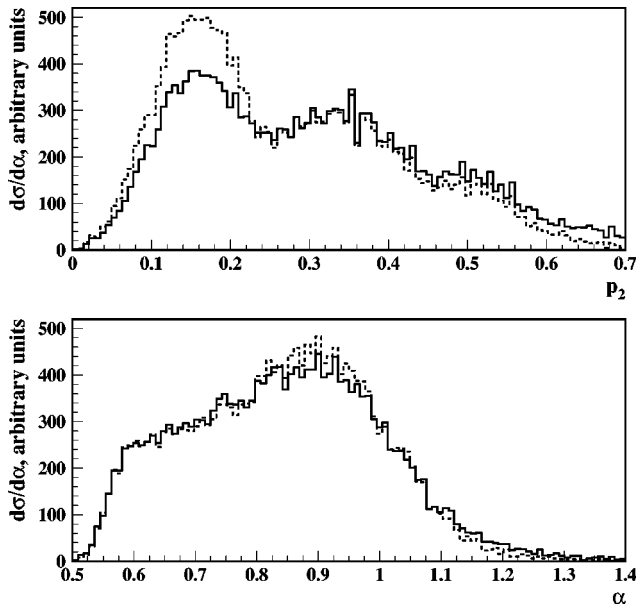

FIG. 10. The p_2 and α dependences of the cross section with and without rescattering with uncorrelated nucleons.

parency. The large contribution from ISI/FSI in the transverse momentum distribution is attributed to the structure of small angle hadronic interaction at high energies. The rescattering is mainly transverse thus affecting mostly the transverse momenta of interacting nucleons.

The above discussion allows us to conclude that the experimental study of the α distribution provides direct information on high-momentum components of the nuclear wave function. On the other hand, the large values of missing transverse momenta are mainly sensitive to the dynamics of initial and final state interactions. In the subsequent sections we will discuss the analysis of the first experimental data on $A(p,2p)X$.

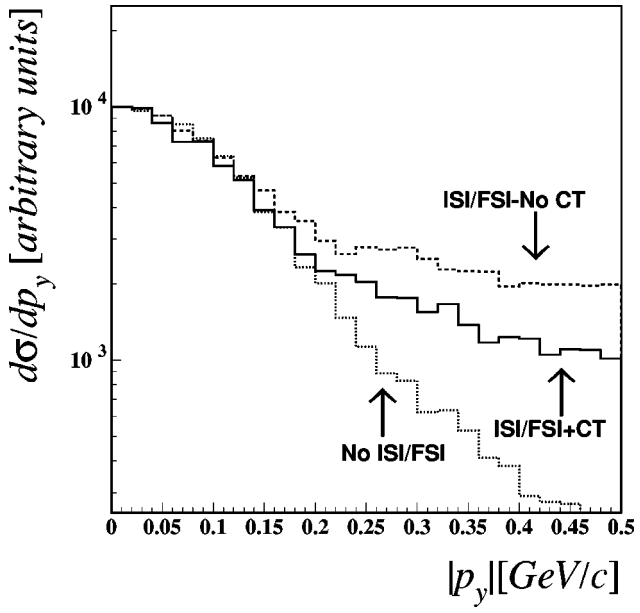

FIG. 11. The p_y dependence of the cross section with and without rescattering effects.

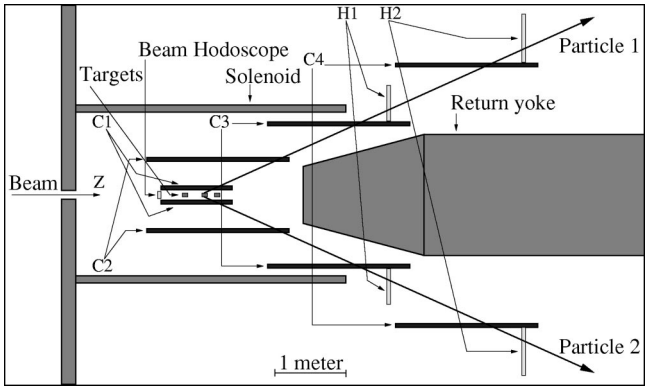

FIG. 12. A schematic view of the EVA spectrometer. $C1-C4$ are the straw tube four layer detectors. $H1$ and $H2$ are scintillator hodoscopes used for fast triggering on high p_t events. The three targets in $C1$ are shown in typical positions. The beam direction (symmetry axis of the detector) is chosen to be the z axis. Not shown in the figure are the beam counters upstream the spectrometer as well as the full iron structure around the solenoid.

IV. MEASUREMENTS AND DATA

We compare the calculations with the data that were collected in EXP 850 using the EVA spectrometer at the AGS accelerator of Brookhaven National Laboratory [12]. In this section we will briefly describe the experiment and the procedures relevant for comparing the data with the calculations.

The EVA collaboration performed a second measurement over a wider kinematical range with incident momenta above 7.5 GeV/c. These data have not yet been analyzed. Some of the calculations in this work are predictions for these new data, which might later become available.

A. The experimental setup

The EVA spectrometer, located on the secondary line $C1$, consisted of a 2-m-diameter and 3-m-long superconducting solenoidal magnet operated at 0.8 T (see Fig. 12). The beam entered along the z axis and hit a series of targets located at various z positions. The scattered particles were tracked by four cylindrical chambers ($C1-C4$, Fig. 12). Each chamber had four layers of long straw drift tubes with a high resistance central wire. For any of the 5632 tubes that fired, the drift time to its central wire was read out. In three out of the four cylindrical chambers, signals were read out at both ends, providing position information along the z direction as well. The information from the straw tubes provided the target identification, the measurement of the particles transverse momentum as they were bent in the axial magnetic field, and their scattering angles. The overall resolution caused by the beam, the target, and the detector were determined from the two-body elastic pp scattering measurement. The standard deviation (σ) for the resolution of the transverse momentum is $\Delta p_t/p_t = 7\%$ and 0.27 GeV/c for the missing energy. The polar angles (θ_3, θ_4) of the two outgoing protons were measured with a resolution of 7 mrad. The beams ranged in intensity from 1 to 2×10^7 over a 1 s spill every 3 s. Two counter hodoscopes in the beam (only one shown in Fig. 12)

provided beam alignment and a timing reference and two differential Cerenkov counters (not shown in Fig. 12) identified the incident particles. Three levels of triggering were used to select events with a predetermined minimum transverse momentum. The first two hardware triggers selected events with transverse momenta $p_t > 0.8$ and $p_t > 0.9$ GeV/c, for the 6 and 7.5 GeV/c measurements, respectively. The third level software trigger required two almost coplanar tracks, each satisfying the second level trigger requirement and low multiplicity hits in the straw tubes. See Refs. [42,43] for a detailed description of the trigger system. Details of the EVA spectrometer are given in Refs. [43–46].

Three solid targets, CH_2, C, and CD_2 (enriched to 95%) were placed on the z axis inside the $C1$ cylinder separated by $\approx$20 c.m. The targets were 5.1×5.1 c.m.^{2} squares and 6.6 c.m. long in the z direction except for the CD_2 target which was 4.9 c.m. long. Their positions were interchanged at several intervals in order to reduce systematic uncertainties and to maximize the acceptance range for each target. Only the C target was used to extract the QE events, while the others served as normalization and reference targets.

B. Event selection and kinematical constraints

Quasielastic scattering events with only two charged particles in the spectrometer were selected. An excitation energy of the residual nucleus $|E_{\rm miss}| < 500$ MeV was imposed in order to suppress events where additional particles could be produced without being detected in EVA. Since this cut is above m_π, some inelastic background, such as that coming from $pA \rightarrow pp\pi^0(A-1)$ events, could penetrate the cuts and had to be subtracted. The shape of this background was determined from a fit to the $E_{\rm miss}$ distribution of events with extra tracks in the spectrometer. An inelastic background with this shape was subtracted. The measured distributions represent background subtracted quantities. See Refs. [46,12] for more details.

The coordinate system was chosen with the z coordinate in the beam direction and the y direction normal to the scattering plane (x,z). The latter was defined by the incident beam and one of the emerging protons. The selection among the two was random. This arbitrariness in the selection did not affect the extracted quantities of interest. The data were analyzed in terms of the momenta in the y direction, p_y, and the light-cone α variable. α was determined with a precision of $\sigma \approx 3\%$. p_y (perpendicular to the scattering plane) had a resolution of $\sigma = 40$ MeV/c. The resolution in p_x (in the scattering plane) was $\sigma = 170$ MeV/c. Because of its better resolution, p_y was used to represent the transverse component.

The laboratory polar angles of both detected protons were limited by a software cut to a region of $\pm 3°$–$5°$ around the center of the angular acceptance, for each target position. The angular range enforced by the software cut was smaller than the geometrical limits of the spectrometer (see Fig. 12) but it ensured a uniform acceptance. Since the experiment was focused on shapes and not absolute values, an acceptance correction in the (θ_3, θ_4) plane was not needed. An explicit cut on the center of mass scattering angle $\theta_{\rm c.m.}$ was not applied on the data, however the cuts on the laboratory polar angles limit the $\theta_{\rm c.m.}$ to the range of 83° to 90° for the ''proton at rest'' kinematics.

C. The longitudinal (α) distributions

Each target position corresponded to a limited polar angular range (θ_3, θ_4) and α is a strong function of $\theta_3 + \theta_4$. To cover the largest possible acceptance in α one had to merge the measured α distributions from different targets. The distributions from the individual target positions were normalized to each other using overlapping regions. The experimental error in each bin includes also the relative normalization error. The value of $|\theta_3 - \theta_4|$ was limited by the largest common acceptance of all target position.

To summarize, the following angular acceptance cuts were applied on the data. (1) $|\theta_3 - \theta_4| < 0.06$ radians (for all target positions and both beam energies); (2) downstream target, $23.5^0 < \theta_3 < 32.0°$ and $23.5° < \theta_4 < 29.5°$ or θ_3 and θ_4 inverted; (3) middle target, $20.0° < \theta_3 < 30.0°$ and $22.0° < \theta_4 < 28.0°$ or θ_3 and θ_4 inverted; and (4) upstream target, $19.0° < \theta_3 < 28.0°$ and $21.0° < \theta_4 < 27.5°$ or θ_3 and θ_4 inverted.

These cuts yield for 5.9 GeV/c the following α acceptance ranges. (1) Downstream target, $0.9 < \alpha < 1.05$; (2) middle target, $0.767 < \alpha < 0.967$; and (3) upstream target, $0.7 < \alpha < 0.867$.

For the 7.5 GeV/c data the angular ranges were as follows. (1) Downstream target, $22.0° < \theta_3 < 32.0°$ and $22.0° < \theta_4 < 31.5°$ or θ_3 and θ_4 replaced; (2) middle target, $21.0° < \theta_3 < 27.0°$ and $21.0° < \theta_4 < 27.0°$; and (3) upstream target, $20.0° < \theta_3 < 26.0°$ and $20.0° < \theta_4 < 26.0°$.

These cuts yield for 7.5 GeV/c the following α acceptance ranges. (1) Downstream target, $0.967 < \alpha < 1.05$; (2) middle target, $0.834 < \alpha < 1.0$; and (3) upstream target, $0.767 < \alpha < 0.934$.

D. The transverse (p_y) distributions

The p_y distributions were studied for narrow regions of α. The regions of α were chosen to yield a large overlap between the 5.9 GeV/c and the 7.5 GeV/c data sets for each target position: (1) $0.74 < \alpha < 0.84$ for the upstream target position; (2) $0.82 < \alpha < 0.92$ for the middle target position; and (3) $0.95 < \alpha < 1.05$. for the downstream target position.

The shapes of the p_y distributions for the two data sets at 6 and 7.5 GeV/c are consistent in each one of the three α regions.

The shapes of the p_y distributions in the three α regions for 6 GeV/c are very similar to those of the 7.5 GeV/c data. Since the data sets of the two energies were found to be consistent, they were added in order to reduce the statistical errors. Even after this procedure the poor statistics for the $0.95 < \alpha < 1.05$ range did not allow us to draw conclusions for this range. All the data presented consist of events that passed all the quasielastic cuts. The residual inelastic background was subtracted in a way similar to that described for the α distributions (see Refs. [12,46] for details). All measured p_y distributions were normalized to 10 000 at $p_y = 0$

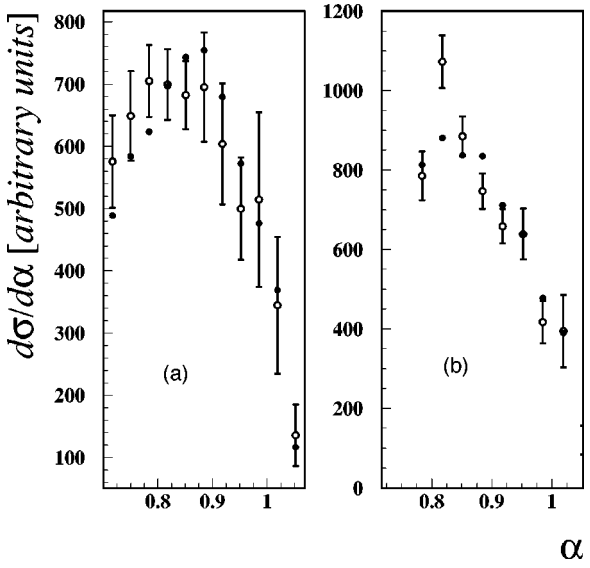

FIG. 13. A comparison between calculated α distributions (●) and the experimental data (○) at 5.9 GeV/c (a) and 7.5 GeV/c (b).

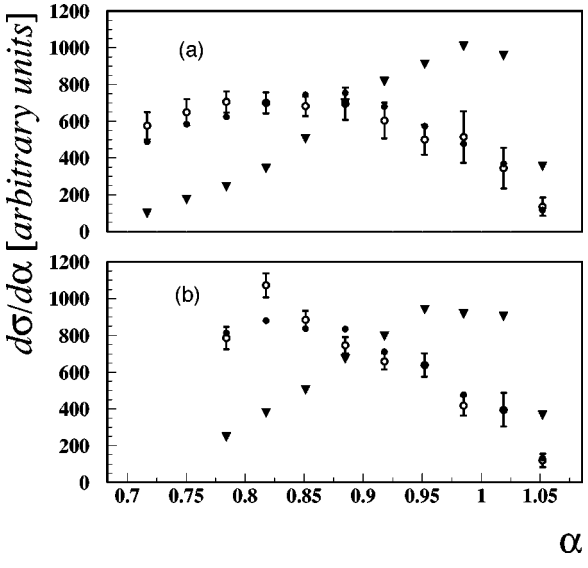

FIG. 14. Calculated longitudinal α distributions with (●) and without (∇) s weighting compared to the measured data (○), at 5.9 GeV/c (a) and 7.5 GeV/c (b).

and all were shown on a logarithmic scale to emphasize their shapes. The data are compared to the calculations in Sec. V.

V. COMPARISON OF THE CALCULATIONS WITH THE DATA

A. The longitudinal (α) distributions

As was mentioned in Sec. III the calculations are implemented through a Monte Carlo code that allows incorporation of the theoretical calculations with the multidimensional kinematic cuts applied in the experiment. The following cuts have been included in the calculations: (1) The angular and α acceptances are constrained for the same ranges as presented in Sec. IV for the data. (2) $60° < \theta_{\rm c.m.} < 120°$ (for all target positions). The calculations include all the described nuclear effects (EMC, ISI/FSI, and CT).

Figure 13 shows the measured longitudinal α distributions at 5.9 GeV/c and 7.5 GeV/c together with the calculations. In the calculation we used the two-nucleon correlation model for the high-momentum component of the nuclear wave function, discussed in Sec. II. For the parameter $a_2(^{12}\mathrm{C})$ which defines the strength of the SRC in the nuclear spectral function [Eq. (9)] we used the value $a_2 \approx 5$ obtained from the analysis of high Q^2 and large Bjorken x $A(e,e')X$ data Ref. [15].

The calculations agree well with the data, $\chi^2 = 0.8$ for 5.9 GeV/c and $\chi^2 = 2.0$ for 7.5 GeV/c.

The next question we ask is whether the data allow us to understand the ingredients contributing to the strength of the α distribution at lower α values.

First, we determine whether the high-momentum-transfer elastic pp scattering off the bound nucleon still follows the s^{-10} energy dependence. In Fig. 14 we compare the calculations using s-independent ''pp cross sections'' (triangle points) and the ''real'' pp cross sections parametrized according to Eq. (10) (solid points). If there were no scaling for hard pp scattering in the nuclei, the α-distribution would peak around $\alpha = 1$, as shown by the calculations with no ''s weighting'' (triangles). The data clearly show a shift to lower α, which confirms the strong s dependence of the quasielastic process.

Next we address the question of whether the strength seen at $\alpha < 1$ comes from SRC in the nucleus. Figure 15 shows two calculated α distributions for the incoming proton momentum of 5.9 GeV/c. One distribution is calculated with the harmonic oscillator wave function only [i.e., $a_2 = 0$, in Eq. (9)] (triangle points). The second distribution is calculated with the SRC contribution to the high-momentum tail of the nuclear wave function, described by $a_2 = 5$ (solid points). These two nuclear wave functions were referred to

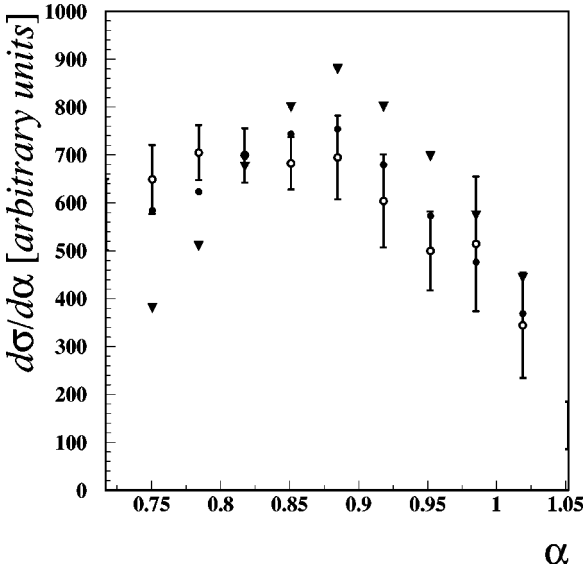

FIG. 15. Longitudinal α distributions for 5.9 GeV/c (○, data; ∇, calculations with $a_2 = 0$; ●, calculations with $a_2 = 5.0$).

as HO and HO+HMC in Fig. 8. The open circles are the data. It is clearly seen in the figure that the α distribution calculated with $a_2=0$ does not provide sufficient strength at low α to describe the data, and SRC contributions are necessary.

It is important to note that both the strong s dependence of hard pp scattering and the contribution of SRC are needed for agreement with the data. A mean field wave function for the nucleus would require a very unreasonable energy dependence of the pp scattering cross section, in order to explain the observed strength of the cross section at $\alpha<1$. Moreover the agreement with the data using the same value of a_2 parameter obtained from electronuclear reactions indicates that we are dealing with a genuine property of the nucleus that does not depend on a specific probe.

B. The transverse (p_y) distributions

As it was discussed in Secs. II and III, we expect the transverse missing momentum of the quasielastic $A(p,2p)X$ cross section to be sensitive mainly to the dynamics of ISI/FSI. The studies of electronuclear $A(e,e'p)X$ reactions, in which FSI occurs through the rescattering of only one knocked-out proton, demonstrated that the eikonal approximation can describe the FSI with better than 10% accuracy (see, e.g., Ref. [47]). This indicates that the expected level of accuracy in calculations of ISI/FSI in $A(p,2p)X$ reactions, in which one incoming and two outgoing protons undergo the soft rescatterings, will be on the order of 15–20 %. Keeping these accuracies in mind, we compare the theoretical calculations with the data checking how well the probabilistic approximation of ISI/FSI can reproduce the shape of the transverse missing momentum distribution.

The following kinematical constraints are imposed in the Monte Carlo calculations: (1) middle target, $0.82<\alpha<0.92$; (2) upstream target, $0.74<\alpha<0.84$; (3) $|\theta_3-\theta_4|<0.06$ rad (for all target positions); and $60°<\theta_{\mathrm{c.m.}}<120°$ (for all target positions). The calculations include all the effects discussed in Secs. II and III (i.e., ISI/FSI, EMC, CT) and the strength of the SRC is calculated with $a_2=5$.

Figure 16 compares between the measured and calculated transverse p_y distributions. Since the theoretical and experimental distributions are normalized to 1000 at the first bin, only the difference in shape between them is relevant. The kinematics correspond to the the combined 5.9 GeV/c and 7.5 GeV/c energies for the upstream target ($\alpha=0.79\pm0.05$). See Sec. IV for the detailed procedure of combining the 5.9 GeV/c and 7.5 GeV/c data sets. We followed the same procedure in the calculations. Figure 17 shows the comparison for the kinematics of the middle stream target ($\alpha=0.87\pm0.05$) similar to Fig. 16.

The calculations presented in Figs. 16 and 17 overestimate the data at the transverse missing momenta above 0.2 GeV/c. There are several reasons for such a discrepancy. First, one should notice that the tail of the distribution above $p_y=200$ MeV/c is only 10% of the peak value at $p_y=0$. Since calculation and the data are normalized at the maximum, even a small discrepancy between calculation and the data at $p_y=0$ will produce a large discrepancy at large values of p_y.

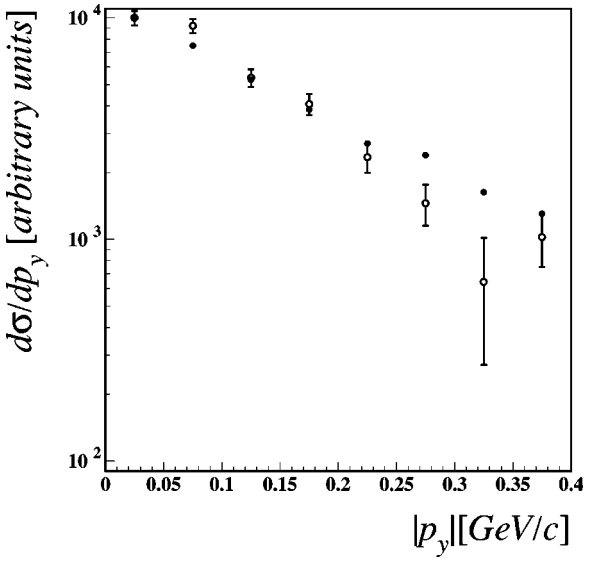

FIG. 16. A comparison between the calculated (●) and experimental (○) p_y distribution combined for 5.9 GeV/c and 7.5 GeV/c momenta. The kinematics for the upstream target with $0.74<\alpha<0.84$ is used (see text for details).

Next, this discrepancy may be the indication of the limit of applicability of the probabilistic approximation of ISI/FSI. In that approximation we neglected the interference terms that may contribute at large values of transverse momenta. Indeed, as the complete calculation of $d(p,2p)n$ reaction demonstrated [29], interference terms are not negligible at $p_t\geqslant 150-200$ MeV/c and their contribution tends to diminish the overall cross section.

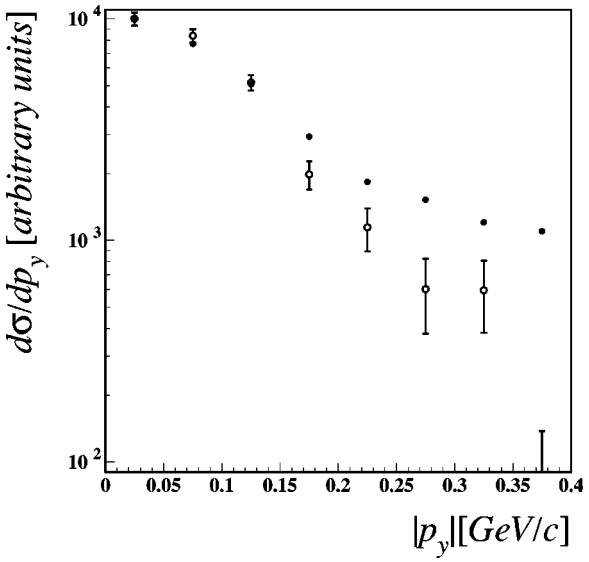

FIG. 17. A comparison of calculated (●) and experimental (○) p_y distributions for combined 5.9 GeV/c and 7.5 GeV/c energies. The kinematics of the middle stream target with $0.82<\alpha<0.92$ is used (see text for details).

Another reason for the discrepancy may be the fact that within the eikonal approximation, starting at transverse missing momenta ($\geqslant 150-200$ MeV/c), the ISI and FSI are dominated by incoherent elastic rescattering which enhance the cross section of the nuclear reaction (see Ref. [48] for details). It was observed in Refs. [49,50] that incoherent elastic rescatterings are much more sensitive to the CT phenomena than the ISI/FSI terms contributing to the nuclear absorption. The qualitative reason is that the absorption is proportional to the total cross section of PLC-N interaction $\sigma^{tot}_{PLC,N}$ while incoherent elastic rescattering is proportional to $(\sigma^{tot}_{PLC,N})^2$. Thus the overestimate of the calculation may indicate that the onset of CT is stronger than that modeled in the calculations (see Sec. II). Note that a noticeable ($\sim$20%) change in the strength of the incoherent elastic rescattering will produce only an $\approx$5% change in the absorption. Thus such a modification of the size of the CT effect will still maintain the agreement of the calculation with the transparency data of Ref. [31].

Ending the above discussion, we can only conclude that the strength of the high transverse momentum distributions is generated by ISI/FSI. However both an improved theoretical calculation of ISI/FSI and a better experimental resolution are needed for understanding the details of the dynamics behind this strength.

VI. SUMMARY

We present a theoretical analysis of the published data on the high-momentum-transfer quasielastic C$(p,2p)X$ reaction.

First, we outline the light-cone plane wave impulse approximation in which the high-momentum component of the nuclear wave function is treated within a two-nucleon short-range correlation model. This work confirms the predictions by Ref. [11] of an α shift of the $A(p,2p)X$ cross section. We further develop the SRC model taking into account the medium modification of the bound nucleon as well as initial and final state reinteractions of the incoming and two outgoing protons in the nuclear medium, combined with color transparency effects.

For nuclear medium modifications we demonstrated that within the color screening model, which describes reasonably the available electroproduction data, the strength of the SRC is not obscured. Furthermore, we demonstrated that in the high-energy regime the α distribution of the bound proton is practically unaltered by ISI/FSI. As a result the α distribution of the C$(p,2p)X$ cross section reflects the genuine distribution of the bound proton in the nucleus. We also demonstrated that the transverse missing momentum distribution is strongly sensitive to the dynamics of initial and final state reinteractions, and we discussed its potential use to study effects related to color transparency.

In addition to the α and p_t distributions we discussed the dependence of the cross section on the total longitudinal momentum of the two outgoing protons. It indicates the existence of a nuclear ''boosting'' effect, in which the sum of the longitudinal momenta of the two outgoing protons is larger than the momentum of the incoming proton. This result is in qualitative agreement with the new data recently obtained at EVA [32].

After briefly describing the experiment, we confront the calculations with the data. The comparison demonstrates that the theoretical expectation of the α shift, based on scaling in hard elastic scattering off a bound nucleon in the nucleus, was correct. The physical meaning of this shift is that hard quasielastic pp scattering is sensitive to the high-momentum components of the nuclear wave function. One observes that a momentum tail in the nuclear wave function, which is needed to explain the data, is significantly larger than can be expected from the mean field approximation. The value of the two-nucleon SRC strength needed to describe the data is in agreement with that obtained from electronuclear reactions. The analysis of the transverse missing momentum distribution shows that it is very sensitive to ISI/FSI and both improved calculations and data are needed for understanding the details of the dynamics that generate the high transverse momentum strength. Thus, studies of the transverse momentum distribution may emerge as an additional tool for studying the color transparency phenomenon.

It is worth emphasizing that the extension of quasielastic studies to higher energies, in which a lower value of α can be probed, (see, e.g., Fig. 2), will provide a new window for investigation of the quark-gluon structure of short-range nucleon-nucleon correlations. In particular, it might enable the experimental investigation if two nearby nucleons will substantially overlap that the quarks from these nucleons can form a multiquark state [51–53]. These configurations would play a dominant role in the determination of the deuteron form factor as $Q^2\rightarrow\infty$ [51]. An important characteristic of these configurations is a large probability of hidden color states [54]. A signature of hidden-color states in hard proton-nucleus scattering will be the large probability of production of Δ isobars, N^*'s and residual nucleons with large excitation energies: $E_{exit}\sim(m_\Delta-m_N)-(m_{N*}-m_N)\approx 300-600$ MeV [52].

ACKNOWLEDGMENTS

Part of the data related to p_y distributions has not been published before. We would like to acknowledge the EVA collaboration for allowing us to present them in this paper. The authors are thankful to the EVA collaboration, especially to the spokespersons S. Heppelmann and A. Carroll, for very useful discussions. Special thanks to J. Alster for many valuable comments and Y. Mardor for providing the details of her analysis of the experimental data. M. Sargsian gratefully acknowledges a contract from the Thomas Jefferson National Accelerator Facility (TJNAF) under which this work was done. TJNAF is operated by the Southeastern Universities Research Association (SURA) under DOE Contract No. DE-AC05-84ER40150. This work was supported also by DOE grants under Contract Nos. DE-FG02-01ER-41172 and DE-FG02-93ER-40771 as well as by the U.S.-Israel Binational Science foundation and the Israel Science Foundation funded by the Israel Academy of Sciences and Humanities.

[1] S.J. Brodsky and G.R. Farrar, Phys. Rev. Lett. **31**, 1153 (1973); Phys. Rev. D **11**, 1309 (1975); V. Matveev, R.M. Muradyan, and A.N. Tavkhelidze, Lett. Nuovo Cimento Soc. Ital. Fis. **7**, 719 (1973).
[2] N. Isgur and C.H. Llewellyn Smith, Phys. Rev. Lett. **52**, 1080 (1984); Phys. Lett. B **217**, 535 (1989).
[3] A. Radyushkin, Acta Phys. Pol. B **15**, 403 (1984).
[4] S.J. Brodsky, C.E. Carlson, and H.J. Lipkin, Phys. Rev. D **20**, 2278 (1979).
[5] G.R. Farrar, S. Gottlieb, D. Sivers, and G.H. Thomas, Phys. Rev. D **20**, 202 (1979).
[6] G.P. Ramsey and D. Sivers, Phys. Rev. D **52**, 116 (1995).
[7] P. Landshoff, Phys. Rev. D **10**, 1024 (1974); P. Landshoff and D. Pritchard, Z. Phys. C **6**, 69 (1980).
[8] J. Botts and G. Sterman, Nucl. Phys. **B325**, 62 (1989).
[9] C. Bourrely and J. Soffer, Phys. Rev. D **35**, 145 (1987).
[10] L.L. Frankfurt and M.I. Strikman, Phys. Rep. **160**, 235 (1988).
[11] G.R. Farrar, H. Liu, L.L. Frankfurt, and M.I. Strikman, Phys. Rev. Lett. **62**, 1095 (1989).
[12] Y. Mardor *et al.*, Phys. Lett. B **437**, 257 (1998).
[13] R. Feynman, *Photon-Hadron Interactions* (Benjamin, Reading, MA, 1972).
[14] L.L. Frankfurt and M.I. Strikman, Phys. Rep. **76**, 214 (1981).
[15] L.L. Frankfurt, M.I. Strikman, D.B. Day, and M. Sargsian, Phys. Rev. C **48**, 2451 (1993).
[16] C. Ciofi degli Atti, S. Simula, L.L. Frankfurt, and M.I. Strikman, Phys. Rev. C **44**, 7 (1991).
[17] S.J. Brodsky and G.F. de Teramond, Phys. Rev. Lett. **60**, 1924 (1988).
[18] D. Sivers, S.J. Brodsky, and R. Blankenbecler, Phys. Rep. **23**, 1 (1976).
[19] L. Frankfurt, E. Piasetzky, M. Sargsian, and M. Strikman, Phys. Rev. C **51**, 890 (1995).
[20] J.J. Aubert *et al.*, EM Collaboration, Phys. Lett. **123B**, 275 (1983).
[21] L.L. Frankfurt and M.I. Strikman, Nucl. Phys. **B250**, 143 (1985).
[22] M.R. Frank, B.K. Jennings, and G.A. Miller, Phys. Rev. C **54**, 920 (1996).
[23] L.L. Frankfurt, M.I. Strikman, and M.B. Zhalov, Phys. Rev. C **50**, 2189 (1994).
[24] R.L. Jaffe, F.E. Close, R.G. Roberts, and G.G. Ross, Phys. Lett. **134B**, 449 (1984).
[25] W. Melnitchouk, M. Sargsian, and M.I. Strikman, Z. Phys. A **359**, 99 (1997).
[26] L. Frankfurt, G.A. Miller, and M. Strikman, Phys. Rev. Lett. **68**, 17 (1992).
[27] I. Mardor, Y. Mardor, E. Piasetzky, J. Alster, and M.M. Sargsian, Phys. Rev. C **46**, 761 (1992).
[28] L.L. Frankfurt, M.M. Sargsian, and M.I. Strikman, Phys. Rev. C **56**, 1124 (1997).
[29] L.L. Frankfurt, E. Piasetzky, M.M. Sargsian, and M.I. Strikman, Phys. Rev. C **56**, 2752 (1997).
[30] M.M. Sargsian, Int. J. Mod. Phys. E **10**, 405 (2001).
[31] A.S. Carroll *et al.*, Phys. Rev. Lett. **61**, 1698 (1988).
[32] A. Leksanov *et al.*, Phys. Rev. Lett. **87**, 212301 (2001).
[33] S. J. Brodsky, in *Proceedings of the Thirteenth International Symposium on Multiparticle Dynamics*, edited by W. Kittel, W. Metzegar, and A. Stergiou (World Scientific, Singapore, 1982), p. 963.
[34] A. H. Mueller, in *Proceedings of the Seventeenth Rencontre de Moriond*, edited by J. Tran Thanh Van (Editions Frontieres, Gif-sur-Yvette, France, 1982), p. 13.
[35] L.L. Frankfurt, G.A. Miller, and M. Strikman, Annu. Rev. Nucl. Part. Sci. **44**, 501 (1994).
[36] P. Jain, B. Pire, and J.P. Ralston, Phys. Rep. **271**, 67 (1996).
[37] G.R. Farrar, H. Liu, L.L. Frankfurt, and M.I. Strikman, Phys. Rev. Lett. **61**, 686 (1988).
[38] L. Frankfurt, G.A. Miller, and M. Strikman, Comments Nucl. Part. Phys. **21**, 1 (1992).
[39] N. Makins *et al.*, NE18 Collaboration, Phys. Rev. Lett. **72**, 1986 (1994).
[40] I. Mardor *et al.*, Phys. Rev. Lett. **81**, 5085 (1998).
[41] J.P. Ralston and B. Pire, Phys. Rev. Lett. **61**, 1823 (1988).
[42] B.K. Jennings and G.A. Miller, Phys. Lett. B **318**, 7 (1993).
[43] J.Y. Wu *et al.*, Nucl. Instrum. Methods Phys. Res. A **349**, 183 (1994).
[44] M. A. Shupe *et al.* Experiment E850 Proposal to Brookhaven National Laboratory, 1988 (unpublished).
[45] S. Durrant, Ph.D. thesis, Pennsylvania State University, 1994.
[46] Y. Mardor, Ph.D. thesis, Tel Aviv University, 1997.
[47] K. Garrow *et al.*, hep-ex/0109027.
[48] D. R. Yennie, in *Hadronic Interactions of Electrons and Photons*, edited by J. Cummings and D. Osborn (Academic, New York, 1971), p. 321.
[49] K.Sh. Egiyan, L.L. Frankfurt, W. Greenberg, G.A. Miller, M.M. Sargsian, and M.I. Strikman, Nucl. Phys. **A580**, 365 (1994).
[50] L.L. Frankfurt, G.A. Miller, W. Greenberg, M.M. Sargsian, and M.I. Strikman, Z. Phys. A **352**, 97 (1995).
[51] S.J. Brodsky and B.T. Chertok, Phys. Rev. Lett. **37**, 269 (1976); **14**, 3003 (1976).
[52] L. L. Frankfurt and M. I. Strikman (unpublished).
[53] V.A. Matveev and P. Sorba, Nuovo Cimento Soc. Ital. Fis., A **45**, 257 (1978).
[54] S.J. Brodsky, C.R. Ji, and G.P. Lepage, Phys. Rev. Lett. **51**, 83 (1983).